Control of noisy chaotic motion in a system with nonlinear excitation and restoring forces

P. E. King
U.S. Bureau of Mines, Albany Research Center, Albany, Oregon 97321

S. C. S. Yim
Oregon State University, Corvallis, Oregon 97331

(Received 10 January 1996; accepted for publication 5 March 1997)

In this study we examine the complex and chaotic oscillations of a dynamical system with nonlinear excitation and restoring forces for the purpose of controlling these oscillatory states. The physical system, modeled as a system of first-order nonlinear ordinary differential equations, takes into account a geometric nonlinearity in the restoring force, a quadratic viscous drag, and a harmonic excitation force. It is controlled using small perturbations about a selected unstable cycle and control is instigated for periodic cycles of varying periodicities. The controller, when applied on the dynamical system with additive random noise in the excitation, successfully controls the system with noise levels in excess of 5% of the total energy, giving the first evidence that (stochastic) control of these systems is possible. © *1997 American Institute of Physics.*
[S1054-1500(97)01102-6]

Sensitive nonlinear dynamics including chaotic oscillatory behavior has been observed in experimental data of a moored, submerged structure. This phenomenon has been verified through analysis and computer simulation of the governing dynamical system. Methods of analyzing system response to harmonic and noisy excitations and subsequent control are needed, should this unpredictability of the observed behavior be deemed undesirable. In this study we present an analysis and control procedure that uses the chaotic response of the system to an advantage. By describing the nonlinear response with unstable periodic orbits (UPOs), a locally linear mapping of the dynamics is obtained. This linear mapping is subsequently employed in a controller design and the controller is applied to the moored structure. Finally, robustness of the controller is investigated under noisy conditions and modifications to the controller are made in order to maintain control of the moored structure under the conditions when noise is present in the excitation. The methods presented are equally applicable to most chaotic systems for which the response time history can be monitored.

I. INTRODUCTION

Recently, chaotic responses have been predicted in a system characterized by a large geometric nonlinearity in the restoring force and viscous drag excitation.[1,2] An example of a system modeled by these types of nonlinearities is a mass moored in a fluid medium subject to wave excitations. These systems include sonars, remote sensors, and data collection devices deployed for mineral exploration, which are of interest to the U. S. Navy and the U. S. Bureau of Mines, are typically suspended by cables from the ocean floor. This class of fluid–structure interaction problems contain highly nonlinear drag and mooring effects. However, despite being of fluid origin, which often indicates infinite dimensionality, the overall effects of the nonlinear fluid loads on the structure can be approximated in terms of an added inertia and a nonlinear coupling of the Morison form. The nonlinear mooring resistance force can be approximated by a low-order polynomial. Hence the resulting mathematical models of these systems are reducible to a low degree system of ordinary differential equations of the Duffing type. This order of approximation is often acceptable for preliminary analysis and design of the types of fluid–structure systems considered (see Refs. 1 and 2 for detailed justifications).

Currently, chaotic motions of moored fluid–structure interaction systems employed by the U. S. Navy and the U. S. Bureau of Mines are not considered in their design. Preliminary analysis of experimental data from such a system has demonstrated the likely presence of chaotic motions in noisy environments.[3] Should the unpredictability of the chaotic behavior observed in these and other associated fluid–structure interaction systems[4,5] be deemed undesirable, methods of analyzing system response to harmonic and noisy excitations and subsequent control of the systems are needed. The analysis and control procedure presented in this study uses the chaotic response to its advantage. By describing the nonlinear response with the unstable periodic orbits (UPOs) of the system, a consistent means of characterizing these strange attractors is obtained.[6–8] This characterization can include the calculation of such invariants as the topological entropy, the Hausdorff dimension,[7] the multifractal spectrum,[9] or the Lyapunov spectrum.[10]

In this study, particular system trajectories are identified and then used to control the chaotic responses. The proposed control method utilizes the local linearity about an unstable cycle to maintain a periodic response within the chaotic operating regime. To maintain stability of the desired periodic response, this method applies a small perturbation about the unstable cycle at discrete time intervals.[11] The proposed

method has been applied successfully to several physical systems, including control of a thermal convection loop[12,13] and the chaotic oscillations in a continuous stirred tank reactor.[14] Other control methods including the use of artificial neural networks for adaptive learning of chaotic oscillations for model reference control of these oscillations has been examined in the cases of chaotic fluid flows[15] and plasmas.[16,17]

In Sec. II we describe the physical system, which includes nonlinear effects of fluid structure interaction as well as nonlinear geometric stiffness. Numerical investigations show that this system possesses periodic, quasiperiodic, and chaotic responses to certain combinations of driving wave amplitudes and frequencies. The regions of chaotic responses are first identified by a semianalytical method of investigating the bifurcation structure and routes to chaos.[2] The analytical predictions are highlighted in Sec. III. This information is used in Sec. IV to numerically investigate chaotic oscillations of the system. In Sec. V the notion of an UPO is introduced and a method of obtaining them is outlined. This method uses only the response time series of the chaotic system and hence is applicable to many systems in which the dynamics are not precisely known *a priori*, but a chaotic time series is available. The ability of the method to identify appropriate unstable cycles in a general chaotic system, and subsequent control of the chaotic responses is investigated in Sec. VI.

The controller utilizes a selected UPO to maintain a trajectory in an oscillatory manner, essentially rendering the system response periodic, even though the system is otherwise operating in a chaotic parameter regime. In Sec. VII we give the results of applying this technique to the nonlinear oscillator defined in the previous sections.

Finally, since the proposed control scheme uses a first-order approximation about an UPO, it is expected that the addition of noise may cause some stability problems with the controller. Several avenues of rendering a robust controller are available; these include filtering the noise and geometric projection. Filtering either assumes prior knowledge of the model (as in Kalman filtering[18]) or it assumes knowledge about the nature of the noise (as in statistical linearization[19]). Geometric projection,[20,21] on the other hand, uses the fuzzy image of the dynamics (via a strange attractor in phase space) to project a trajectory back onto the original phase space. However, in this study, a modification of the controller is employed to obtain the desired robustness. This modification extends the method in the case when noise is present and is discussed in Sec. VIII.

II. SYSTEM WITH GEOMETRIC AND HYDRODYNAMIC NONLINEARITIES

Figure 1 shows a system moored by cables in a fluid medium. The fluid itself is undergoing motion and an associated excitation force is described by the forcing function $F(\ddot{x},\dot{x},t)$, where $\dot{x}=dx/dt$ and $\ddot{x}=d\dot{x}/dt$. With restraints for vertical and rotational motion, this system is modeled as a single-degree-of-freedom system for the surge, x.[2] The (nonlinear, second-order ordinary differential) equation of motion is derived by using the fact that the system is hydrodynamically damped with external forcing. The forcing excitation is modeled as the sum of a constant current and an oscillatory wave term. Because the cables are thin and the dimensions of the mass are small compared to the orbital motions of the wave particles, the fluid–structure interaction can be modeled accurately by use of the small-body theory, which assumes that the presence of the structure does not influence the wave field. This implies that the waves flowing past the structure do not change due to the fluid–structure interaction. The mooring angle produces a geometric nonlinearity in the restoring force that can become highly nonlinear for $b=0$, a two-point system, or nearly linear for $b \gg d$ for the four-point system. The equation of motion for this system is given by Refs. 1 and 2 as

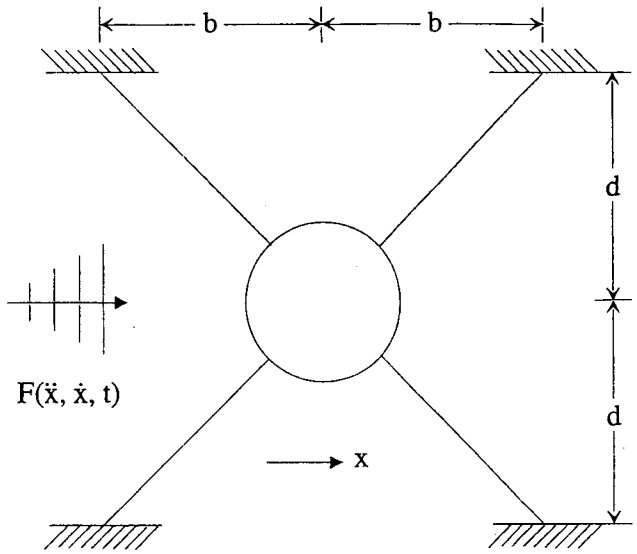

FIG. 1. A moored system suspended by cables and subject to current and wave excitation.

$$m\ddot{X}+c\dot{X}+R(X)=F(\ddot{X},\dot{X},t), \tag{1a}$$

where the nonlinearities are contained in the restoring force R and the excitation force F. The restoring force describes the geometric configuration of the mooring lines and assumes linear elastic behavior so that the nonlinearity is strictly due to the geometric configuration of the system. The restoring force can be shown[2] to have the form

$$R(X)=k[X+b\ \mathrm{sgn}(X)]\left(1-\sqrt{\frac{d^2+b^2}{d^2+[X+b\ \mathrm{sgn}(X)]^2}}\right), \tag{1b}$$

where $\mathrm{sgn}(X)$ is the signum function defined by

$$\mathrm{sgn}(X)=\begin{cases}+1, & \text{for } X>0,\\ 0, & \text{for } X=0,\\ -1, & \text{for } X<0.\end{cases}$$

The excitation force is a combination of viscous drag and inertial components based upon the interactions between the moored structure and the fluid medium. This excitation force is modeled by

$$F(\dot{X},\dot{X},t)=\lambda(u-\dot{X})|u-\dot{X}|+\mu(\dot{u}-\ddot{X})+\rho\bar{V}\dot{u}. \tag{1c}$$

The system parameters are given by the system mass m, damping c, and line stiffness k. λ and μ are the hydrodynamic viscous drag and added mass, ρ is the fluid density, $\bar{V}$ is the displaced volume of fluid, $u=u(t)$ is the fluid particle velocity under current and waves given by $u(t)=u_0+u_1\sin(\omega t)$, and $u_1=u_1(a,\omega)$.

Assuming the structure does not alter the fluid flow, performing an equivalent linearization on the quadratic drag force and normalizing, a dimensionless first-order autonomous nonlinear differential equation can be obtained:

$$\begin{aligned}\dot{x}&=y,\\ \dot{y}&=-R(x)-\gamma y+F(y,x,\theta),\\ \dot{\theta}&=\omega,\end{aligned} \tag{2a}$$

where $x=X/d$ and the resulting nonlinear restoring force becomes

$$R(x)=\psi[x+\beta\ \mathrm{sgn}(x)]\times\left(\frac{1}{\sqrt{1+\beta^2}}-\frac{1}{\sqrt{1+[x+\beta\ \mathrm{sgn}(x)]^2}}\right), \tag{2b}$$

and the excitation force is given by

$$F(y,x,\theta)=f_0-f_1\sin(\theta). \tag{2c}$$

The appropriate dimensionless constants are defined by

$$\psi=\frac{k}{m+\mu},\quad \beta=\frac{b}{d},\quad \gamma=\frac{c+\lambda_1}{m+\mu}, \tag{2d}$$

and the constants f_0 and f_1 depend upon the hydrodynamic characteristics of the system. Although at first glance this system appears to be significantly more complex than the simple nonlinear systems presented in standard texts, e.g. Nayfeh and Mook,[23] it turns out that the fluid–structure system possesses nonlinear response properties very similar to those of the Duffing system.[1,2]

III. ANALYTICAL PREDICTIONS

Numerical simulations of the response of the structure in the fluid medium have been shown to exhibit periodic, quasiperiodic, and chaotic responses in surge motion, as depicted in Fig. 1. This response has been verified through an analytical treatment of Eqs. (2a)–(2c). In this analysis, a Hamiltonian approach is employed to examine the fundamental geometric nonlinearity and a harmonic-balance method[22,23] is used to investigate the frequency response characteristics of the primary, sub- and superharmonics.[23] A variational approach is also employed to identify a bifurcation structure and routes to chaos of the model.[1,2]

The associated Hamiltonian[24] of the system described by Eqs. (2a)–(2c) is obtained by neglecting the damping term

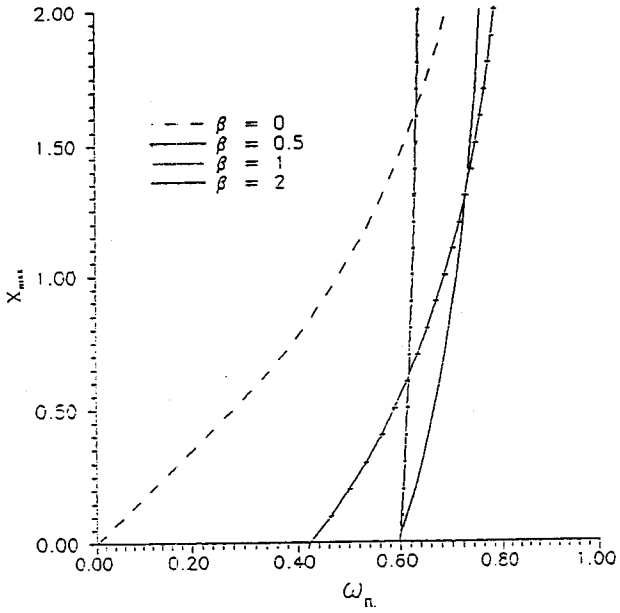

FIG. 2. Degree of geometric nonlinearity as a function of the mooring angle.

(by setting $\gamma=0$) and the forcing term ($F\equiv 0$). From this formulation, the natural period, T_n, of the Hamiltonian is computed from the natural period, $T_n=2\pi/\omega_n$, where

$$\omega_n=\frac{\pi}{2}\left(\int_0^{x_{\max}}\frac{dx}{y(x)}\right)^{-1}, \tag{3}$$

$$y(x)=\sqrt{2}(V(x_0)-V(x))^{1/2}\equiv\dot{x}, \tag{4}$$

and $V(x)$ is the potential energy and is given by

$$V(x)=\psi\left(\frac{x^2}{2}-\tau(\sqrt{1+(\beta+x)^2}+\sqrt{1+(\beta-x)^2})\right). \tag{5}$$

Equation (3) characterizes the geometric nonlinearity and is sometimes called the frequency response (or backbone) curve.[23] The curvature of the backbone curve shows the degree of nonlinearity. For a weak nonlinearity the curvature is near zero and the backbone curve resembles a vertical line. For a strong nonlinearity the curvature is positive for a stiffening system and negative for a softening system. This is exhibited in Fig. 2, which gives the result for Eqs. (2a)–(2c) for the stiffening case. As can be seen, the mooring angle creates a strong nonlinearity for $\beta=0$ and a weak nonlinearity for $\beta\gg 1$.

The harmonic balance[22,23] method of approximating a solution to the system [Eqs. (2a)–(2c)] is applied to study the frequency response characteristics of the resonance modes. The method assumes an approximate solution of the form

$$x_0(t)=\sum_{k=0}^{M}A_k\cos(k\omega t+\phi_k), \tag{6}$$

where M is the order of the approximation and A_k is the amplitude of the kth harmonic. This approximate solution is then substituted into the original equations and the resulting expressions are rearranged and squared. By equating the harmonic terms and the constant terms separately to zero, a set

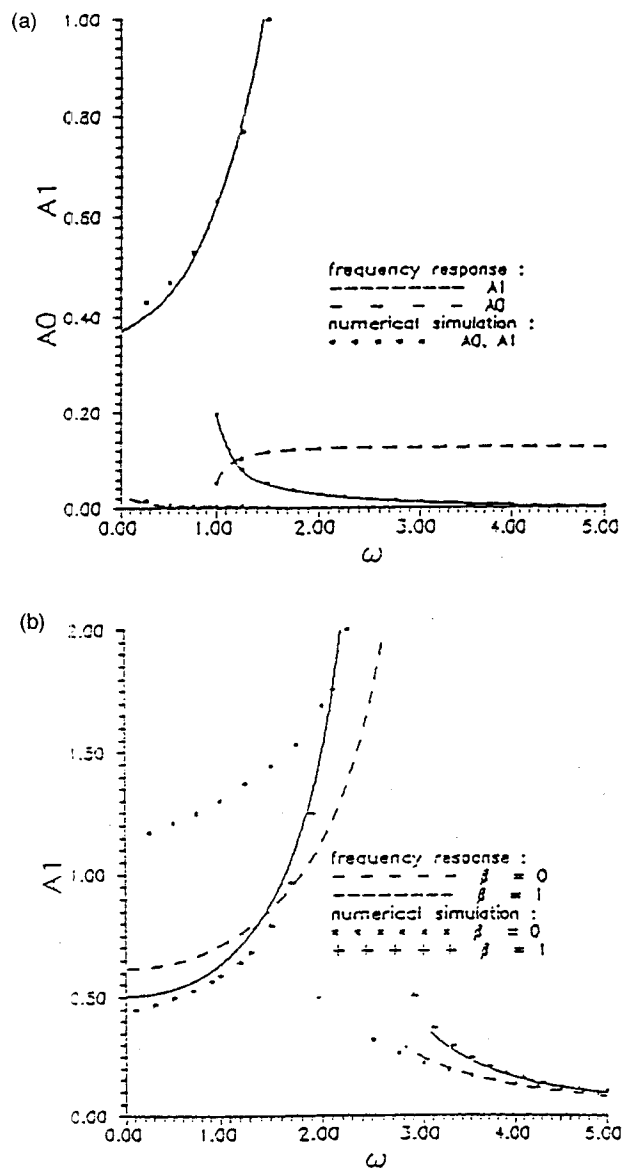

FIG. 3. Frequency response curves subject to (a) current and wave excitation ($\gamma=0.5$, $\psi=10.0$, $f_0=0.01$, $f_1=0.1$) and (b) wave excitation alone ($\gamma=0.01$, $\psi=10.0$, $f_0=0.0$, $f_1=2.0$).

of nonlinear algebraic equations in the A_k's and ϕ_k's is obtained and subsequently solved using standard procedures.[22] Figure 3 shows the zeroth- and first-order amplitude as a function of frequency. As is evident, this system exhibits a jump phenomena as the frequency is swept through the values shown.[23]

The system bifurcations are identified by considering a perturbed solution of the form $x(t)=x_0(t)+\epsilon(t)$, where $x_0(t)$ is an approximate solution and $\epsilon(t)$ represents a small perturbation. Substituting this into Eqs. (2a)–(2c) and linearizing the resulting expression yields

$$\ddot{\epsilon}+\gamma\dot{\epsilon}+\psi H[x_0(t)]\epsilon=0, \tag{7a}$$

where γ and ψ are defined in Eq. (2d) and the periodic function H is given as follows:

$$H(x_0)=(1+\beta^2)^{-1/2}-\{1+[x_0+\beta\ \mathrm{sgn}(x_0)]^2\}^{-3/2}. \tag{7b}$$

Performing a Fourier series expansion on H produces a generalized Hill's equation[23] of the form

$$\ddot{\epsilon}+\gamma\dot{\epsilon}+\psi H[\theta]\epsilon=0, \tag{8a}$$

for

$$H[\theta]=\frac{a_0}{2}+\sum_n a_n\cos(n\theta). \tag{8b}$$

Note that Eqs. (8a)–(8b) define parametric excitation and resonant interaction, where harmonics of all orders are possible. The use of Floquet theory (described in detail in Ref. 23) gives the particular solution to the variational equation as

$$\epsilon(t)=\exp(\zeta t)Z(t), \tag{9}$$

where the real part of the constant ζ determines the stability of the approximate solution, and the complex part of ζ corresponds to the natural frequency of the periodic response. The function Z is periodic in T, i.e., $Z(t)=Z(t+T)$.

By investigating the order of the harmonic part of the solution the sub- and superharmonic solutions can be determined. The procedure is conducted by examining the symmetric solution $Z(t)=Z(t+T/2)$ or the period-doubled solution $Z(t)=Z(t+2T)$. The boundaries of the stability regions can be obtained by performing a harmonic-balance approximation to the Hill's variational equation (8a) at the stability limits, where $d\zeta/dt=0$. (Specific details of the solution procedure can be found in Ref. 2, while a description of the general procedure can be found in Ref. 23.) For the fluid–structure interaction systems of interest to the U. S. Navy and the U. S. Bureau of Mines, preliminary experimental results have indicated that the primary resonance is of major concern.[3] Although, the analysis procedures described in this study are equally applicable to higher-order resonances, primary resonance will be employed for demonstration purposes.

The above analysis yields the frequency response curve of the primary resonance, $Z(t)=Z(t+T)$, given by

$$\omega^2=\frac{1}{2a_0}\left[\psi(a_0^2-a_1^2)-\gamma^2 a_0 \pm\sqrt{\gamma^4 a_0^4+2\psi\gamma^2(a_1^2-a_0^2)+\psi^2(a_1^2-a_0a_1)^2}\right]. \tag{10}$$

Note that in Eq. (10), $\gamma\ll 1$. For the undamped system, $\gamma=0$, and $\omega\approx\sqrt{(\psi a_0/2)}$. The distribution of the a_i's and their influence on system behavior had been examined.[1,2]

Similarly, the stability boundaries for the $\frac{1}{2}$ subharmonic can also be obtained by inserting the period-doubled solution $x_{1/2}(t)=b_{1/2}\cos(\theta/2)$ [corresponding to $Z(t)=Z(t+2T)$] into Eq. (8a). This yields the frequency response curve

$$\omega^2=2(\psi a_0-\gamma^2\pm\sqrt{\gamma^4-2\psi\gamma^2 a_0+\psi^2 a_1^2}). \tag{11}$$

Now, the regions of bifurcations can be approximated by observing that the intersections of the frequency response curves obtained from Eq. (6) and the investigations of the stability regions that lead to the frequency response curves

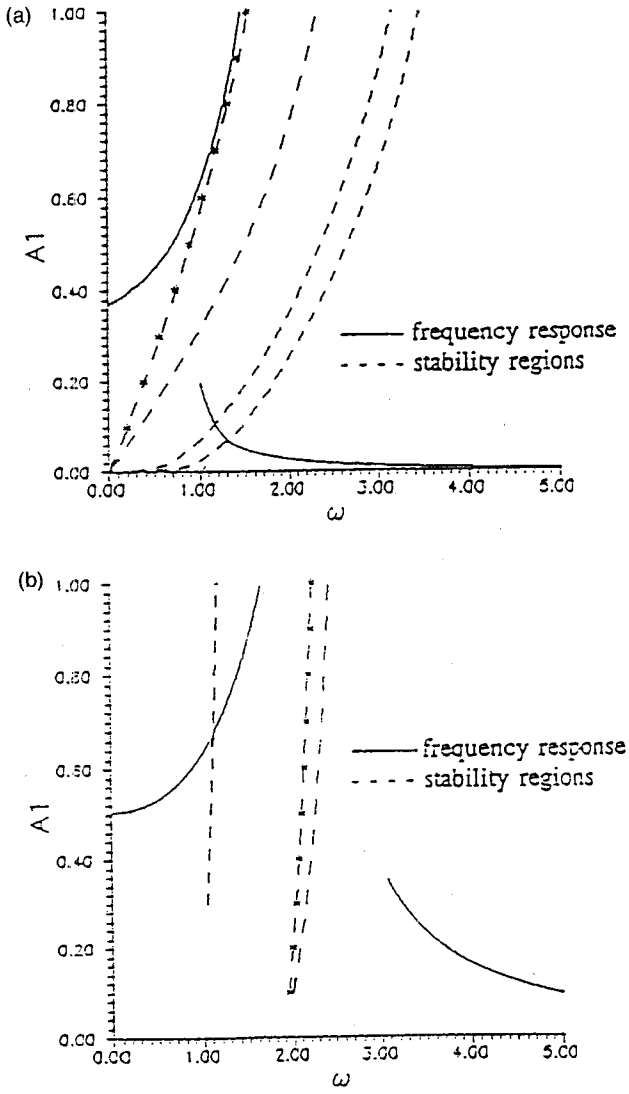

FIG. 4. Stability diagrams of the system with linearized excitation for (a) current and wave excitation ($\gamma=0.01$, $\psi=10.0$, $\beta=0.0$, $f_0=0.01$, $f_1=0.1$) and (b) wave excitation alone ($\gamma=0.01$, $\psi=10.0$, $\beta=1.0$, $f_0=0.0$, $f_1=2.0$).

given by Eqs. (10)–(11), as shown in Fig. 4. From this analysis, obviously the strength of the geometric nonlinearity (as evidenced by β) plays an important role in the ultimate response of the system. In fact, by examining the frequency response characteristics and equating them with the stability regions a period-doubling bifurcation structure is obtained.

IV. NUMERICAL INVESTIGATIONS

The analytical investigations above provide a guide for a numerical search in parameter space for various types of responses including the existence and coexistence of periodic solutions, period-doubling bifurcations, and chaos. Extensive numerical investigations and many examples as presented in Ref. 2, show that Eqs. (2a)–(2c) exhibit periodic, quasiperiodic, and chaotic motions. These motions were verified through the analytical predictions discussed above. As a demonstration, Fig. 5 shows one of the many possible cha-

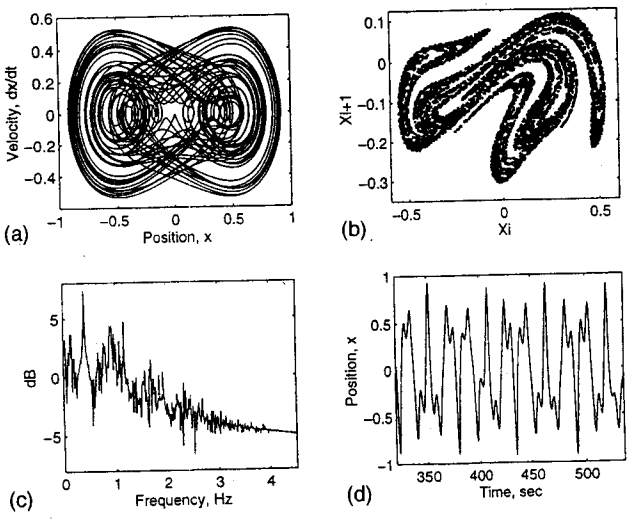

FIG. 5. Chaotic response of the nonlinear system with parameter values $\omega=0.335$, $\gamma=0.01$, $\psi=4.0$, $\beta=0.0$, $f_0=0.0$, and $f_1=2.0$ exhibiting the (a) chaotic attractor, (b) Poincaré section, (c) power spectrum, and (d) time history of the (surge) position.

otic responses of the system, where the parameter values used were $\omega=0.335$, $\gamma=0.01$, $\psi=4.0$, $\beta=0.0$, $f_0=0.0$, and $f_1=2.0$. In the chaotic regime, this system exhibits both steady-state chaos and transient chaos, where the system undergoes a transient chaotic response before it settles into periodic or quasiperiodic oscillations.[2] Figures 5(a)–5(d) show the phase space portrait, Poincaré section, frequency spectrum, and a typical time series, respectively, of a chaotic response. The Poincaré sections are obtained by stroboscopically sampling the time series every $2\pi/\Gamma$ and plotting the points sequentially, i.e. by plotting $x(t)$ vs $x(t+\Gamma)$ for Γ the sampling period. One can notice the fractal structure of the Poincaré section. The presence of an abundance of these complex harmonic responses predicted by the analytical and numerical results indicate that their influence on extreme and fatigue designs of the fluid–structure interaction systems may need to be included in the future.

V. UNSTABLE PERIODIC ORBITS

The numerical simulations together with the analytical results show that the oscillatory nature of Eqs. (2a)–(2c) exhibit a range of modes, including periodic, sub- and superharmonics and chaotic motions. A means of analyzing the chaotic motion by using the time series alone has been introduced by Refs. 6 and 7. The procedure utilizes the unstable periodic orbits of a system. Since a chaotic attractor contains a multitude of UPOs of varying periodicities, much of the nonlinear characteristics can be identified through these special cycles. It is well known that UPOs are dense in a chaotic attractor,[9,11] and, in fact, this is a necessary condition for chaos to exist.[26] This fact is exploited in the following discussions.

The basic idea behind the use of an UPO is that if the chaotic system is allowed to evolve long enough, then a trajectory will return arbitrarily close to a given unstable cycle, arbitrarily often. This is because these cycles are dense on

the attractor and that they are periodic and yet unstable. Thus, if the system is on a cycle it will remain on it for all time. However, if there is any minute deviation from the cycle, then the chaotic trajectory will diverge from this unstable cycle. Because of the "mixing" property of the chaotic attractor, some time later the trajectory will again come arbitrarily close to this UPO.

In other words, suppose that a chaotic time series $x(t)$ is available. Let $\eta>0$ be given, then at some time t in the time series $|x_p-x_t|<\eta$, that is the chaotic trajectory has come arbitrarily close to the UPO, x_p, of period p. At some time Γ later $|x_p-x_{t+\Gamma}|<\eta$ and the trajectory has come close to the UPO again. To identify the unstable cycle of period p, a search through the dataset for all points separated by Γ time steps that are a distance of η apart is performed. To ensure that the points obtained by this search correspond to a particular unstable cycle and not another nearby unstable cycle; not only are the points that are identified used but also their images under integration (or iteration for discrete systems). This is done by restricting the points of interest to those with iterates of which are within $\delta>\eta$ of each other, $|x_{p+1}-x_{t+1}|<\delta$. That is, all points such that $|x_p-x_t|<\eta$ and $|x_p-x_{t+\Gamma}|<\eta$ are considered and that $|x_{p+1}-x_{t+1}|<\delta$ to ensure that only one cycle is included and not several nearby cycles.

In practice, this is typically performed on a Poincaré section where the continuous flow is mapped to a discrete iterative dynamical system of one less degree of freedom. Let Z_i be a point on the Poincaré section and suppose Z_p is an unstable periodic point on the section representing the UPO of period p. Then, the algorithm for calculating the UPO consists of searching the dataset on the section, $\{Z_i\}_{i=1}^{N}$, for all points that are within η of Z_p the set $\{\xi_i:|Z_p-Z_i|<\eta\}$. Once these points have been identified, their corresponding image, or next iterate, is investigated. The set of points whose images (i.e., the next iterates) are within δ, $|Z_p-Z_{i+p}|<\delta$, for some $\delta>\eta$, are considered to correspond to that UPO, otherwise they correspond to a different UPO and are not further examined.

The last step is to identify the stability characteristics of the UPO, which is performed by using a least-squares procedure to calculate a linear map, A, which maps Z_i to Z_{i+p}, where Z_i and Z_{i+p} correspond to the periodic point Z_p. This is accomplished by creating the vectors $D=\{d_i\}$ and $E=\{e_i\}$, where the d_i's are the deviations of the points from the UPO under consideration, $d_i=Z_i-Z_p$, and the e_i's are the deviations of the iterates from the image of the UPO, $e_i=Z_{i+\Gamma}-Z_{p+\Gamma}$. The point corresponding to the UPO, Z^*, is taken as the centroid of points under consideration.

The linear map A (an $n\times n$ matrix, where n is the dimension of the Poincaré section, usually taken as 2) is calculated by a least-squares method that minimizes the error orthogonal to the approximate solution of the matrix equation $\|DA-E\|^2$, which, since D and E are vectors, has a solution given by $A=\text{inv}(D^TD)D^TE$.[25] The stability characteristics of the UPO are governed by the eigenvalues of the map A

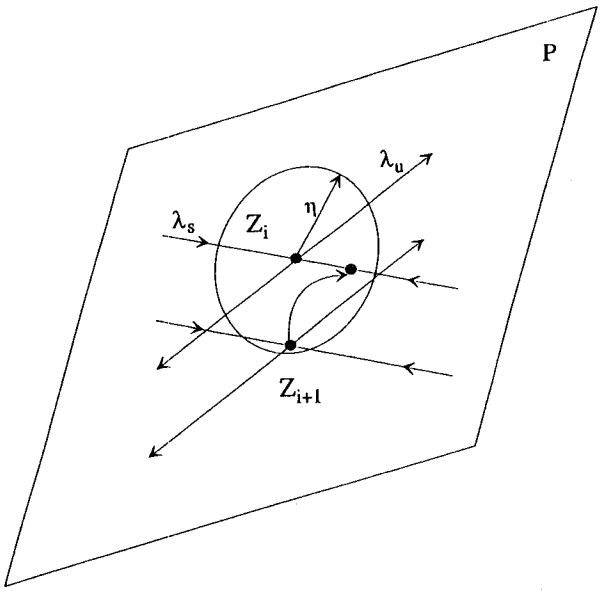

FIG. 6. Schematic of the action of the controller on a point. The control law pushes the point Z_{i+1} towards the stable eigenvector of Z_i.

VI. CONTROL OF CHAOTIC SYSTEM RESPONSES

Once a periodic cycle has been selected for control and the corresponding linear map A has been calculated, control of the system about an unstable cycle can be maintained by applying a small perturbation to the chaotic trajectory about the UPO on the Poincaré plan. That is, the system is allowed to oscillate chaotically until the first time the trajectory enters within the η ball of the chosen UPO. Once within this ball, a small perturbation in the direction of the stable eigenvector of the linear map can be applied to ensure that upon the next return to the Poincaré section the trajectory is still within η of the UPO. Figure 6 is a schematic of this operation in which the point Z_{i+1} is perturbed toward the stable eigenvector of the UPO.

A means of finding the magnitude and direction of the perturbation is obtained by employing the pole placement method,[27,28] which is a state feedback rule devised to render the eigenvalues of the controlled system stable. A linear map describing the evolution of a trajectory from a point close to a periodic point on the Poincaré section to its next iterate is calculated as before. It remains to find a feedback rule, which, when added to the linearized system, renders the nonlinear system stable.

Consider the dynamical system (linearized within the η ball as in Sec. V) represented by the state-space system,

$$\dot{x}=Ax+By, \tag{12a}$$

where x is the response of the system, y is the external forcing, A is the linear mapping, and B is a column vector. Suppose that the external forcing can be written as $y=y_c+y_e$, where y_c describes a control input and y_e is the usual external excitation. Next, consider a feedback law of the form $y_c=-K^Tx$, then Eq. (12a) can be rewritten as

$$\dot{x}=(A-BK^T)x+By_e. \tag{12b}$$

Now, the homogeneous portion of Eq. (12b) determines the linear systems natural behavior, hence if the external excitation is ignored and the subscript from y_c is dropped, then a feedback of the form $y=-K^T x$ can be considered and Eq. (12b) takes the form

$$\dot{x}=(A-BK^T)x. \tag{13}$$

The goal is to find a vector K^T such that the eigenvalues of the matrix $(A-BK^T)$ are asymptotically stable[28,29] (i.e., $|\lambda_i|<1$ for $i=1\cdots n$). This ensures that the fixed points of the associated system, Eq. (12b), are stable. The eigenvalues of the matrix $(A-BK^T)$ are called the regulator poles while the problem of placing these poles in an appropriate spot on the complex plane is called the pole placement problem.[30] The solution to this problem lies in the fact that one is free to choose K^T in an advantageous way, as long as the eigenvalues have the appropriate characteristics. If the system given by the pair (A,B) is controllable, then a solution to the pole placement problem always exists.[27] It can be shown that (A,B) is controllable when the $n\times n$ controllability matrix, C, has full rank, for the controllability matrix defined by

$$C=[B|AB|A^2B|\cdots|A^{n-1}B], \tag{14}$$

and where the columns of C are made up of the column vectors $B,AB,A^2B,\ldots,A^{n-1}B$. The control law then consists of picking the entries in the vector K^T, called gains, so that the roots of the characteristic equation [Eq. (15)] are in prescribed positions. Since the λ_i's are known, this amounts to choosing the c_i's in the characteristic polynomial $\pi(\lambda)$:

$$\begin{aligned}\Pi_{A-BK^T}(\lambda)&=\det[\lambda I-(A-BK^T)]\\&=(\lambda-\lambda_1)(\lambda-\lambda_2)\cdots(\lambda-\lambda_n)\\&=c_n+c_{n-1}\lambda+\cdots+\lambda^n.\end{aligned} \tag{15}$$

A general method for calculating the c_i's is given by Ackerman's formula for pole placement in Ref. 30. The idea is to transform the pair (A,B) into controllable canonical form[27] by constructing a particular transformation matrix, solving for the gains in terms of the controllable canonical form and then transforming back. The result yields the choice of gains as $K^T=(-\sigma_n+c_n,\ldots,-\sigma_1+c_1)G^{-1}$, where $G=C\Lambda$ is the transformation matrix, C is the controllability matrix, and Λ has the form[27,28,30]

$$\Lambda=\begin{bmatrix}\sigma_{n-1} & \sigma_{n-2} & \cdots & \sigma_1 & 1\\ \sigma_{n-2} & \sigma_{n-3} & \cdots & 1 & 0\\ \vdots & \vdots & & \vdots & \vdots\\ \sigma_1 & 1 & \cdots & 0 & 0\\ 1 & 0 & \cdots & 0 & 0\end{bmatrix}. \tag{16}$$

The c_i's are the coefficients of the characteristic polynomial $\pi_{A\text{-}BK^T}(\lambda)$ and the σ_i's are the coefficients of the characteristic polynomial $\pi_A(\lambda)$. For the case where A is 2×2, it can be shown that an optimal choice (in the sense of time to control) for the gain vector is $K^T=[\lambda_u,-\lambda_u\lambda_s]$, where λ_u is the unstable eigenvalue and λ_s is the stable eigenvalue of A.[11,23]

One can now formulate an algorithm to control a chaotic system utilizing this control law on a Poincaré section. First, the linear map, A, of an unstable cycle is constructed as before and its eigenvalues identified. Then, setting $x=Z_i-Z^*$ and $\dot{x}=Z_{i+1}-Z^*$ in Eq. (13) yields the control law for the discrete UPOs on the Poincaré section as

$$Z_{i+1}=(A-BK^T)(Z_i-Z^*)+Z^*. \tag{17}$$

Then, calculating the eigenvalues of A, λ_u, and λ_s, choosing $K^T=[\lambda_u,-\lambda_u\lambda_s]$, and applying Eq. (17) whenever the trajectory comes within η of Z^* on the Poincaré section yields the desired stable characteristics. The final point left to consider is a relative distance on the Poincaré section a trajectory can be from Z^* and still be able to guarantee that the controller will perform adequately. The answer to this lies in the fact that since it was required that $|Z^*-Z_{i+1}|<\delta$ by construction then, combining this with Eq. (17) yields

$$|Z_i-Z^*|<\frac{\delta}{|A-BK^T|}. \tag{18}$$

Since K^T was constructed to render the eigenvalues of the matrix $A-BK^T$ stable, and $(A-BK^T)^{-1}$ exists, this defines an area of width $2\delta/|A-BK^T|$ about Z^*, for which the control should be applied.

VII. APPLICATION OF CONTROL TO A MOORED STRUCTURE

Consider the chaotic oscillations of Eqs. (2a)–(2c) for the parameter values given as before ($\omega=0.335$, $\gamma=0.01$, $\psi=4.0$, $\beta=0.0$, $f_0=0.0$, and $f_1=2.0$) exhibited in Figs. 5(a)–5(d). A search was done on the Poincaré data exhibited in Fig. 5(b) to obtain all points that were near a period-1 orbit. This is done by comparing all points Z_i that are close and whose next iterate Z_{i+1} are also close (where the Z_i's are taken by stroboscopically sampling the position, x). Then, the UPO of period 1 is estimated as the mean of the set of points found to correspond to it (cf. Sec. V). Utilizing this method, the system structural response data found a UPO of period 1 at the values $Z^*=[x,\dot{x}]^T$, where $x=0.2623$ and $\dot{x}=-0.0677$. A linear map is constructed that maps the points near the UPO Z^* toward Z^* along the direction of the stable eigenvector, as seen in Fig. 6. In this case the linear map is given by

$$A=\begin{bmatrix}0.8793 & 0.2766\\ 0.4553 & -0.0729\end{bmatrix}, \tag{19}$$

which has a practically neutrally stable eigenvalue $\lambda_u=0.9970$ and a stable eigenvalue $\lambda_s=-0.1906$. If the feedback control is applied only to the position x, this gives

$$B=\begin{bmatrix}1\\0\end{bmatrix}. \tag{20}$$

Choosing the gain vector $K^T=[\lambda_u,-\lambda_u\lambda_s]$ yields the control poles at $p_{1,2}=[-0.2951,0.1044]$. Thus, each time the system trajectory crosses the Poincaré section near Z^* the controller affects this point by applying the control law, Eq. (17), ensuring that the trajectory returns near the point

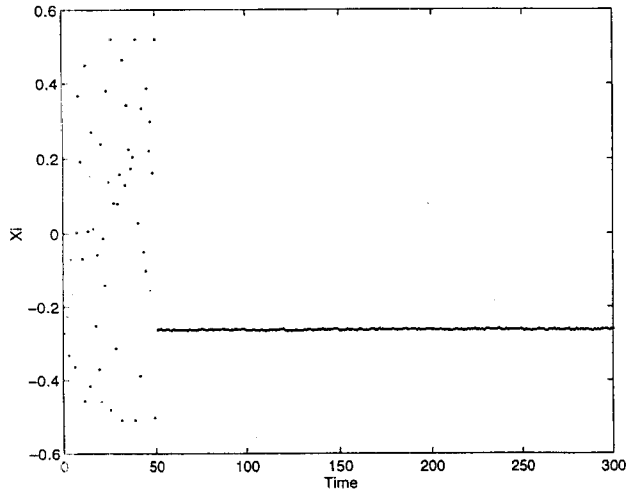

FIG. 7. Example of controlling the system about a period-1 cycle showing the Poincaré points versus time before and after control is applied.

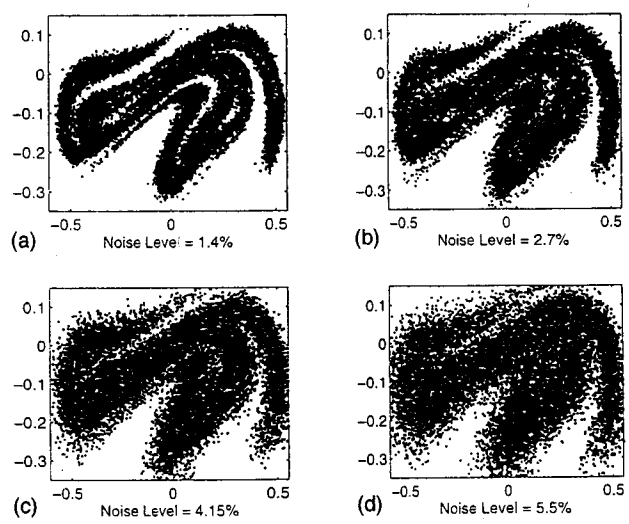

FIG. 9. Effects of increasing noise on the Poincaré portraits.

Z^* on the next return to the Poincaré section. The results of this application are shown in Fig. 7, which is a plot of the Poincaré points versus time, exhibiting the controlled periodic oscillation after an arbitrary duration of chaotic oscillations.

To further demonstrate the effectiveness of this strategy, a higher-order periodicity is identified and the controller is again applied. Analysis of the higher-order motions, and in particular period-3 motion, is very similar to that of the primary resonance case treated in Sec. III (and has been examined in detail in Refs. 1 and 2 and, hence, is not reported here). Figure 8 shows the results of this calculation for a period-3 orbit identified at the point $Z^*=[x,\dot{x}]^T$ for x $=-0.3609$ and $\dot{x}=0.0359$. The linear map obtained for this case is given by

$$A=\begin{bmatrix} 0.9904 & -0.113 \\ -0.097 & -0.145 \end{bmatrix}, \tag{21}$$

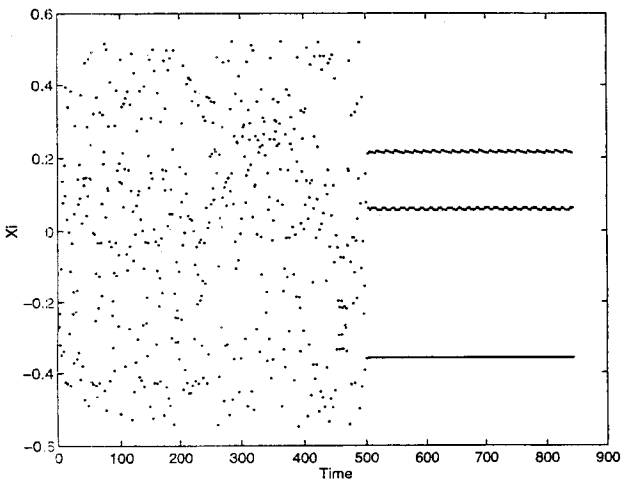

FIG. 8. Example of controlling the system about a period-3 cycle.

which has neutrally stable and stable eigenvalues $\lambda_u=1.000$ and $\lambda_s=-0.1544$, respectively. The controller poles are placed at $p_{1,2}=[-0.6177,0.2068]$ and the controller, Eq. (17), is again applied to initiate control each time the system trajectory intersects the Poincaré section near the UPO at Z^* with period 3. The system oscillates chaotically until the trajectory comes close to the period-3 UPO, at which time the controller is applied and subsequently the system oscillates between the period-3 points.

Observe that, despite the complexity of the dynamics between points in time where control is applied, the method produces a desired periodic motion through small adjustments. This method works well for arbitrary chaotic time series. The algorithm to control this chaotic system is to first obtain enough Poincaré points to be able to characterize an unstable periodic orbit, typically a minimum of 20 points. Once the unstable orbit is identified, a linear map is obtained by a least-squares minimization of the matrix equation involving the points near the UPO and their iterates. Given this map, a feedback law is postulated that places the control poles in a stable operating regime. Finally, the system is allowed to oscillate until the trajectory enters within η of the UPO. At this time, control is applied to produce the desired periodic orbit.

VIII. CONTROL OF SYSTEM WITH NOISE

The benefit of using small perturbations to control a deterministic nonlinear dynamical system within the chaotic operating regime has been presented above. However, for a typical real physical system such as a moored fluid–structure system, there will be noise added to the system through measurement errors as well as a random component in the excitation. For example, Fig. 9 shows the Poincaré map of the noisy chaotic response obtained by adding (band-limited) white noise of finite variance to the excitation term in the deterministic case [as shown in Fig. 5(b)]. Here, the noise energy content is increased from 1.4% [Fig. 9(a)] to 5.5% [Fig. 9(d)] of the forcing energy. In this case a series of

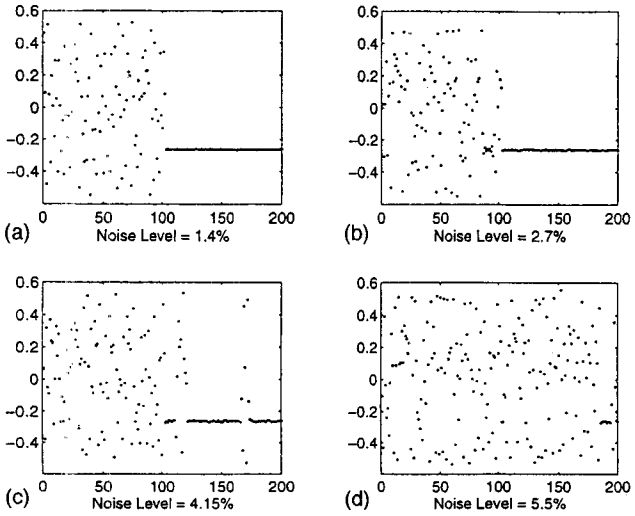

FIG. 10. Effects of increasing noise on the controller in Fig. 7.

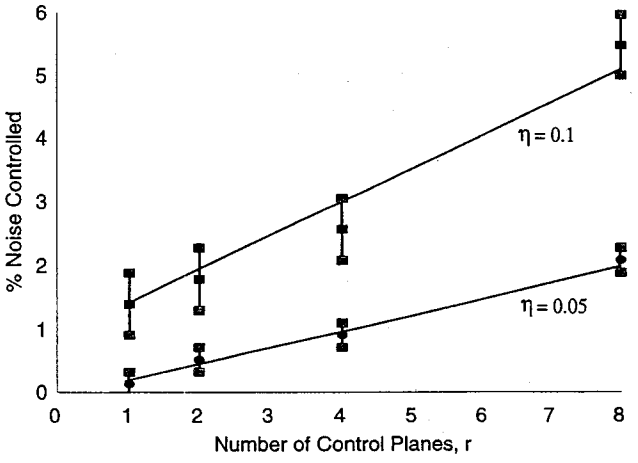

FIG. 12. Effects of the increasing number of control sections on the increasing amounts of controllable noise for several control tolerances.

Poincaré sections about the chaotic attractor can be constructed by stroboscopically sampling every $2\pi/r\Gamma$, where r is the number of sections desired. This yields r separate controllers evenly distributed throughout the cycle, thus decreasing the long term effects of the noise with respect to an individual controller. By applying the above control scheme on each Poincaré section, the UPO can be targeted from one section to the next. If these sections are selected appropriately, then the effects of noise can be minimized.

Figure 10 shows the results of adding the white noise to the excitation term in the period-1 example above. Here, the noise energy level is increased from 1.4% to 5.5% of the forcing energy to exhibit the effects of the noise on the controller without making any modifications to the control scheme. Figures 10(a)–10(d) are the Poincaré points from the controlled system as the noise is increased. Observe that, as the noise level is increased from 0% to 5.5%, the system goes from being completely controlled, to a mode where the controller appears to be effective only during limited durations, and finally to the point where the effects of noise overpowers the influence of the controller. For the system and example considered, the controller appears to have an acceptable performance with no modifications for up to 2.7% noise energy.

A simple modification to the control scheme can dramatically increase the controllability of the system. By taking several Poincaré sections around a single cycle, and then building a feedback controller on each section, the effects of the noise are reduced proportionally to the number of sections the controller is applied on per cycle.

Figure 11 shows the results of the previous example with four control sections. Each of the four sections has been created by sampling the same time series dataset at four times the rate of that in Fig. 10, $r=4$. Then, using the scheme outlined above, a linear map on each section is constructed, finally, each time a trajectory crosses a section within the control tolerance, Eq. (17) is applied for that section. Figure 11 shows the results for one of the sections and the varying noise levels. With four control sections, an increase from 2.7% to 4.15% noise can be acceptably controlled.

The number of control sections versus the amount of noise that the system controller is able to handle are shown in Fig. 12. Here, two levels of control influence, i.e. two different values of η (0.05 and 0.1), are employed. It is assumed that the system is fully controlled if it can be controlled for 100 Poincaré points (or about 85 000 time series data points). Figure 12 indicates an approximately linear relationship between the controllable level of the energy of the noise versus the number of sections required for complete control.

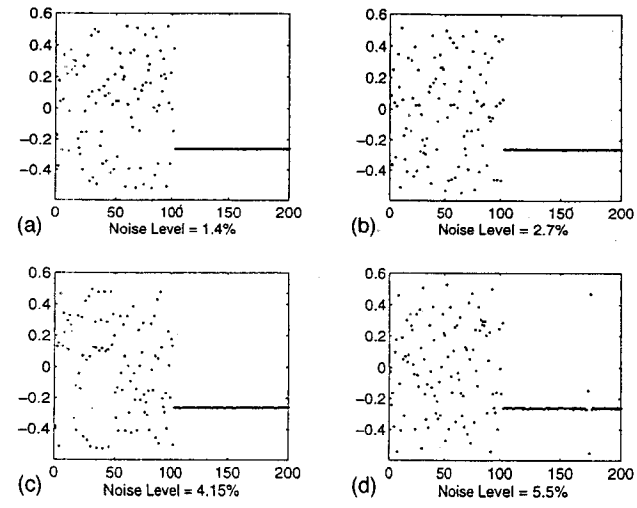

FIG. 11. Control of noisy chaos when control is applied on four control sections, and the noise levels go from 1.4%–5.5%.

IX. CONCLUDING REMARKS

In this study we examine control of the chaotic oscillations of a fluid–structure interaction system. The system un-

der consideration, although of fluid origin, is modeled as a low degree of freedom system by considering cases for which the small-body theory applies. This assumes that the structure does not influence the wave field, allowing for the nonlinear fluid loads to be approximated in terms of an added inertia and a nonlinear coupling. This, together with restraints on vertical and rotational motion and, by approximating the nonlinear mooring resistance with a low-order polynomial, yields the desired low-order system.

The nonlinear dynamics of the fluid–structure interaction system have been demonstrated to exhibit chaotic oscillations under certain environmental conditions and verified on data obtained from experiments. This fact is used to an advantage in the design of a controller. This study outlines a method for controlling chaotic systems, in general, with the use of the systems dynamics and small perturbations. The method uses a chaotic time series to categorize unstable periodic orbits. This is done by mapping the time series to a Poincaré section and then obtaining the unstable periodic orbits through an exhaustive search of the Poincaré points. This produces a linear map for which the pole placement method of feedback control can be applied. The method was first applied to the model to verify control. Then, the method was applied to the model in the case that band-limited white noise of finite variation was added to the excitation term, producing the first indications that (stochastic) control of moored systems is possible.

An unstable periodic point can be identified by realizing that after p iterations (where p is the periodicity of the cycle), a trajectory will return to a neighborhood of its corresponding unstable cycle. By investigating all of the points that are a small distance apart after every p iterates the set of UPOs of period p can be obtained.

Given an UPO of period p, control can be applied by taking advantage of the local linearity of the UPO. A linear map is constructed from the set of points about the periodic cycle and then the stability of this map is investigated. The controller uses the pole placement procedure to perturb a trajectory toward the periodic cycle along the stable direction of the linear map. This ensures that the linear system dynamics are locally stable and system control is achieved. This control amounts to small perturbations to the system trajectory at prescribed times to maintain the desired oscillatory characteristics. The control algorithm is then applied to the fluid–structure interaction system. The controller was able to stabilize the chaotic oscillations of the system about periodic orbits of arbitrary periodicity. As examples, the control of a period-1 orbit and a period-3 orbit were demonstrated.

An extension of the system was investigated to achieve a more robust controller under the circumstances that additive noise is present in the excitation force. This extension applies the same algorithm of control design to a series of Poincaré sections produced by stroboscopically sampling every $2\pi/r\Gamma$, where r is the number of sections desired. This yields r separate controllers evenly distributed, thus decreasing the long term effects of the noise with respect to an individual controller. This method appears to yield a linear growth in the amount of noise that the system is able to handle. More robust control schemes will be examined in the near future.

Finally, should the responses of the prototypes corresponding to the model tests mentioned in the beginning of this study confirm the existence of chaotic motions in the (noisy) field environments, the analysis and control method presented in this study can be applied to suppress these motions if desired. Extensions of this study to the multi-degree-of-freedom physical models and subsequent design of practical controllers for experimental tests are being examined.

ACKNOWLEDGMENTS

The authors wish to acknowledge the financial support of the U.S. Bureau of Mines process control-program (AL-92-A-001) and the United States Office of Naval Research (Grant No. N0001-92-J-1221).

[1] O. Gottlieb and S. C. S. Yim, "Deterministic motions of nonlinear mooring systems. Part I: analysis and predictions," Ocean Engineering Report No. OE-93-02, Oregon State University, Corvallis, OR, 1993.
[2] O. Gottlieb and S. C. S. Yim, "Onset of chaos in a multi-point mooring system," *Proceedings of the 1st (1990) European Offshore Mechanics Symposium*, Trondheim, Norway, 20–22 August 1990, pp. 6–12.
[3] S. C. S. Yim, M. A. Myrum, O. Gottlieb, H. Lin, and I. M. Shih, "Summary and preliminary analysis of nonlinear oscillations in a submerged mooring system experiment," Ocean Engineering Report No. OE-93-03. Oregon State University, Corvallis, OR, 1993.
[4] S. C. S. Yim and H. Lin, "Chaotic behavior and stability of free standing offshore equipment," Ocean Eng. **18**, 225–250 (1991).
[5] S. C. S. Yim and H. Lin, "Nonlinear impact and chaotic response of slender rocking objects," J. Eng. Mech. **117**, 2079–2100 (1991).
[6] D. P. Lathrop and E. J. Kostelich, "Characterization of an experimental strange attractor by periodic orbits," Phys. Rev. A **40**, 4028–31 (1989).
[7] D. Auerbach, P. Cvitanovic, J.-P. Eckmann, G. Gunaratne, and I. Procaccia, "Exploring chaotic motion through periodic orbits," Phys. Rev. Lett. **58**, 2387–2389 (1987).
[8] P. Cvitanovic, "Invariant measurement of strange sets in terms of cycles," Phys. Rev. Lett. **61**, 2729–2732 (1988).
[9] C. Grebogi, E. Ott, and J. A. Yorke, "Unstable periodic orbits and the dimensions of multifractal chaotic attractors," Phys. Rev. A **37**, 1711–1724 (1988).
[10] M. Sano and Y. Sawada, "Measurement of the Lyapunov spectrum from a chaotic time series," Phys. Rev. Lett. **55**, 1082–1085 (1985).
[11] E. Ott, C. Grebogi, and J. A. Yorke, "Controlling chaos," Phys. Rev. Lett. **64**, 1196–1199 (1990).
[12] J. Singer, Y.-Z. Wang, and H. H. Bau, "Controlling a chaotic system," Phys. Rev. Lett. **66**, 1123–1125 (1991).
[13] Y. Wang, J. Singer, and H. H. Bau, "Controlling chaos in a thermal convection loop," J. Fluid Mech. **237**, 479–498 (1992).
[14] V. Petrov, V. Gaspar, J. Masere, and K. Showalter, "Controlling chaos in the Belousov–Zhabotinsky reaction," Nature, **361**, 240–243 (1993).
[15] C. J. Einerson, H. B. Smartt, K. L. Moore, and P. E. King, "Modeling and control of nonlinear chaotic systems using a feedforward neural network," *Intelligent Engineering Systems Through Artificial Neural Networks*, edited by C. H. Dagli, L. I. Burke, and Y. C. Shin (ASME, New York, 1992), Vol. 2.
[16] P. E. King, T. L. Ochs, and A. D. Hartman, "Chaotic responses in electric arc furnaces," J. Appl. Phys. **76**, 2059–2065 (1994).
[17] P. E. King, A. D. Nyman, T. L. Ochs, and C. J. Einerson, "Modeling for control of an electric arc furnace using a feedforward artificial neural network," in *Intelligent Engineering Systems Through Artificial Neural Networks*, edited by C. H. Dagli, L. I. Burke, B. R. Fernández, and J. Ghosh (ASME, New York, 1992), Vol. 3.
[18] B. D. O. Anderson and J. B. Moore, *Optimal Filtering* (Prentice–Hall, Englewood Cliffs, NJ, 1979), p. 357.
[19] J. B. Roberts and P. D. Spanos, *Random Vibration and Statistical Linearization* (Wiley, New York, 1990), p. 407.

[20] R. Cawley and G.-H. Hsu, "Noise reduction for chaotic data by geometric projection," in *Applications of Digital Image Processing XV*, edited by A. G. Tescher, Proc. SPIE **1771**, 368–376 (1993).
[21] R. Cawley and G.-H. Hsu, "Another new noise reduction method for chaotic time series," in *Proceedings of the 1st Experimental Chaos Conference*, 1–3 October 1993, edited by V. Arlington, S. Vohra, M. Spano, M. Shlesinger, L. Pecora, and W. Ditto (World Scientific, Singapore, 1992), pp. 38–46.
[22] D. W. Jordan and P. Smith, *Nonlinear Ordinary Differential Equations*, 2nd ed. (Clarendon, Oxford, 1987), p. 381.
[23] A. H. Nayfeh and D. T. Mook, *Nonlinear Oscillations* (Wiley, New York, 1979), p. 704.
[24] S. Wiggins, *Introduction to Applied Nonlinear Dynamical Systems and Chaos* (Springer-Verlag, Berlin, 1990), p. 672.
[25] G. Strang, *Introduction to Applied Mathematics* (Wellesley–Cambridge Press, Wellesley, MA, 1986), pp. 37–38.
[26] R. Devaney, *An Introduction to Chaotic Dynamical Systems* (Addison–Wesley, Reading, MA, 1987), p. 320.
[27] R. A. DeCarlo, *Linear Systems, A State Variable Approach with Numerical Implementation*, Prentice–Hall, (Englewood Cliffs, NJ, 1989), pp. 335–345.
[28] F. J. Romeiras, C. Grebogi, E. Ott, and W. P. Dayawansa, "Controlling chaotic dynamical systems," Physica D **58**, 165–192 (1992).
[29] G. Nitsche and U. Dressler, "Controlling chaotic dynamical systems using time delay coordinates," Physica D **58**, 153–164 (1992).
[30] G. F. Franklin, J. D. Powell, and A. Emami-Naeimi, *Feedback Control of Dynamic Systems*, 2nd ed. (Addison–Wesley, New York, 1991), pp. 377–396.